Charge Transport and Accumulation around a Spacer Insulator for Application in HVDC Wall Bushing

Qingying Liu[1] and **Jiu Dun Yan**[1]
[1]Department of Electrical Engineering and Electronics
The University of Liverpool
Liverpool, L69 3GJ, the United Kingdom

and **Liucheng Hao**[2], **Bo Zhang**[2], **Shan Liu**[3]
[2]Pinggao Group Co. Ltd
State Grid Corporation of China
Pingdingshan City, Henan Province, 467001, P. R. China

[3]Department of Electrical Engineering,
Tsinghua University,
Beijing, 100084, P. R. China

ABSTRACT

A charge transport model based on ion drift in gases of strong electron affinity has been studied in details and validated against experimental results in air and SF_6 at different pressure and voltage levels. The size of the insulators also differs significantly. The choice of the model parameters, i.e. the solid and gas material properties, is carefully examined with information from existing literature. Results show that using the selected parameters, satisfactory agreement between predicted and measured potential distribution and surface charge density along the insulator surface can be obtained. Computational results for an 1100 kV epoxy spacer for use in HVDC wall bushing show that the concept of electrical conductivity as a material property is no longer valid in strong electric field for the gas surrounding the insulator. The polarity and density of the accumulated surface charge depend on the relative largeness of the electrical conductivity of the insulator material and the effective conductivity of the gas. The nonlinear effect due to ion generation and recombination becomes significant at very high voltage. The metallic cap providing shielding of the triple junction at the high voltage end of the insulator can induce much stronger local electric field near the insulator surface, by a factor of 1.48, if its shape is not optimized against the insulator geometry.

Index Terms — HVDC insulation, HVDC spacer, epoxy insulator, charge transport, surface charge accumulation

1 INTRODUCTION

DC power generation and distribution first appeared in 1882 at 110 V. However, it lost to AC technology in the War of Currents around 1890 largely because there was no practical means to transform the DC voltage. As a result, AC technology dominated the electricity industry over the next 100 years and the transmission voltage level increased steadily to 750 kV in 1965 [1] and has reached 1100 kV nowadays [2]. Although DC technology was used in specific applications, its voltage level remained around 100 kV until 1970 [3]. The availability of semi-conductor power electronics components led to the revolutionary increase in DC transmission voltage levels, jumping to 400 kV in 1970 [4], which was then followed by a renewed interest and exploitation of HVDC transmission technology. More than 20 lines have already been installed at a voltage level of 800 kV at relatively long transmission distances. Most of the lines above 750 kV were installed in the past ten years [5].

While HVDC is advantageous over HVAC for the transmission of bulk volume of electricity over long distance (>700 km), the behaviour of solid insulators is more complicated than those used in HVAC applications due to the phenomenon of charge accumulation on the interface of gas-solid insulation. Insulators are used to provide mechanical support to conductors of significant weight and electrical insulation between the conductor and the earth. They are made of materials with low electrical conductivity (like epoxy or cast resin) to minimise the leakage current. Insulators often represent the weakest point in the insulation system.

The earliest paper, to the authors' knowledge, that suggested the importance of surface charge accumulation was by Cooke [6]. It is commonly recognised that the accumulation of surface

charge may affect the flashover characteristics of supporting insulators under HVDC stress [6-9]. However a comprehensive literature review shows that only a very limited amount of quantitative evidence exists to demonstrate the significant reduction of DC insulation strength in terms of flashover voltage under the influence of long term charge accumulation [9-12]. In these published works charges were deliberately generated by corona discharge to manifest the role of accumulated charges.

The initiation of a surface flashover is usually through the emission of electrons from the triple junction or localised ionization near the insulator surface where the electric field is much enhanced. In practice, the flashover voltage of supporting insulators is determined by a number of factors, such as the shape and structure of the spacer, contamination of surface increasing the local electric field strength or surface conductivity [13, 14], defects or protrusions on the surface [15-17], or attachment of metallic particles on the surface. There was also work showing that material impurity and electrode profile can become purely responsible for the accumulation of surface charge while the type of gas and insulation material yet play a less important role in the accumulation process [8,18]. Therefore, at present the long-term insulation behaviour of insulators under HVDC stress is indeed an extremely complicated problem and not well understood. Appropriate models will be needed to assist the explanation of the operational behaviour of HVDC insulators and to minimise the adverse effect that can occur in reality.

A significant amount of work exists either on 1) the measurement of electrostatic potential distribution or surface charge density on insulator surface under DC stress, or 2) the interpretation of the experimental results using charge transport models. The earliest work was most done by Japanese researchers [7,9,17,19,20] with focus on the measurement of surface potential distribution of model insulators in SF_6 Gas Insulated Switchgear (GIS). It was confirmed in the above work that surface charge density is in the range of 2-5 nC/cm^2 when a voltage of 200 kV was applied for a long duration (139 hours). It was suggested that surface charge density rapidly increased in several tens of minutes following the voltage application, and finally approached a saturated state in 3-5 hours [9]. The maximum applied voltage was 310 kV on a rod insulator with a length of 38.9 mm placed in SF_6.

More recent work on measurement was reported by a German group [21,22]. The potential distribution along the surface of an epoxy insulator with Al_2O_3 filler was measured for up to 8000 hours in air when a constant DC voltage was applied. The measurement was corrected for possible influence due to the presence of the probe itself. The insulator has a typical length of 132 mm and diameter of 80 mm. The maximum applied voltage was 15 kV. Results show that the potential profile along the insulator surface changes gradually with the application time of the DC voltage. The maximum voltage drop of 5 kV takes place at a location on the surface that is close to the high voltage electrode (at 80% of the insulator length from the earthed end). This is significant in view of the effect of the accumulated charges. The maximum surface charge density was obtained with a value of 1.75 nC/cm^2 after 25,000 hours. This is probably the most complete and reliable set of measurement results with all conditions given.

On the modelling side, the earliest interpretation of charge measurement was based on Maxwell's equations applied in a single direction [6], i.e. in the normal direction of the insulator surface. The role of positive and negative ions drifting and diffusing in gases of strong electron affinity such as SF_6 and air was recognised early in 1980 [6]. A model including charge transport in gas was first proposed by Wiegart in 1988 [23] but a more complete charge transport model was only recently applied to model the experimental cases [21,22,24]. Different values of the model parameters, such as the bulk electrical conductivity of solid insulation material, ion pair generation rate, mobility of ions and recombination coefficient, were used in different work, accounting for the difference in materials used (due to impurity or filler material) and thermodynamic conditions of the gas. Encouraging results have been obtained on insulators at voltage levels up to 400 kV [24] with different insulator shapes and sizes, but no verification of the simulation results is given. There has been more model verification work recently but its focus is on the time-evolution of the field distribution [25, 26]. The model based on ion transport in gas will therefore need to be further tested and improved for use in practical product design which must consider the insulator behaviour with design imperfection and realistic operation conditions.

The present work aims at further verification of the charge transport model based on available experimental results from different sources and the application of the model to study the main features of the charge accumulation process around a full scale supporting spacer that is designed for use in 1100 kV HVDC wall bushings. Section 2 describes the mathematical model and boundary conditions based on consideration of the physical processes. The accuracy of the numerical solution of the governing equations and its dependence on mesh size is also discussed in Section 2. The modelling of two experimental cases is performed in Section 3 where prediction based on the model is compared with experimental results in details. The charge transport behaviour of a supporting spacer is studied in Section 4 and conclusions finally drawn in Section 5.

2 THE MATHEMATICAL MODEL FOR CHARGE TRANSPORT

There has been experimental evidence showing that following the application of a DC voltage, an insulator will undergo a transient process (capacitive field) before a steady state is reached where electrical conductivity controls the distribution of electric field. The flow of charge in gaseous or solid media during the transient process leads to the accumulation of charges that subsequently affects the electric field distribution. As a result, conduction current is adjusted to finally reach a situation where conservation of charge is fulfilled.

2.1 GOVERNING EQUATIONS

Because of the high electrical conductivity of the electrode material and low leakage current through the insulator, the potential drop in the electrode is negligibly small. The potential equation is therefore not solved in the electrode part. The flow of charges in solid insulation material such as epoxy under the

action of an applied electric field is controlled by its electrical conductivity. The ability to conduct depends on the energy band structure of the material [27] and the number of electrons in the conduction band, which is a material property. Therefore, the current density satisfies the following equation

$$\nabla \cdot (\sigma_{Vs} \nabla \varphi_s) = 0 \quad (1)$$

where σ_{Vs} is the volume electrical conductivity which in practice depends on the material, the fillers and the casting process. φ_s is the electrostatic potential. The relative permittivity of epoxy can be chosen in the range of 2.5-5 [17,24,28]. It was reported in [28] that the bulk conductivity of epoxy material varies with the applied electric field

$$\sigma_{Vs} = \sigma_0 \cdot e^{\alpha \cdot E} \quad (2)$$

where σ_0 and α are both empirical coefficients relating to the resin material and casting technology. However, both coefficients can take values over a wide range, $10^{-19} - 10^{-12} S/m$ for σ_0 and $0.015 - 0.1\, m/MV$ for α. The same authors measured the conductivity of GIS-utilized epoxy resins with alumina and silica fillers. Their results show that the conductivity varies insignificantly over 0 to 6 kV/mm and its average value is 2×10^{-14} S/m for fillers of Al_2O_3 and SiO_2. For field strength larger than 11 kV/mm, an average value of 8×10^{-13} S/m was obtained. No guidance is given on the selection of these two coefficients for commercial grade materials.

Other experimental evidence [17] shows that the bulk conductivity remains constant at 10^{-14} S/m for untreated epoxy specimen when the applied field strength lies in the range of 1kV/mm to 5 kV/mm. In more recent modelling work [21], a value of 3.33×10^{-18} S/m was chosen to obtain results that agree well with measurements. Given the large difference of its value in literature, the bulk electrical conductivity of epoxy insulator with or without fillers should be obtained by measurement if reliable prediction based on a charge transport model is to be obtained. For the work in Section 4, a constant value of 1.6×10^{-16} S/m, which was measured at 20°C with an electric field strength of 2.8×10^7 V/m, i.e. 28 kV/mm, is provided by the manufacturer and used in the modelling work.

The ability of gas to conduct current depends on the number density of charged particles and their collision frequency with other particles. In weak electric field, the number density of charged particles is controlled by their local generation and loss rate due to ionization and recombination and the drift of charged particles in electric field does not influence the number density remarkably. Thus, the concept of electrical conductivity is valid. However, in strong electric field, the influence of charge drift becomes significant and the number density of charged particles varies remarkably in space, as will be shown in Section 4. The electrical conductivity of the gas can no longer be treated as a material property. Thus, it is necessary to consider the transport processes of charged particles.

Electrons generated by ionization are slowed down to thermal energies within some tens of picoseconds [23]. Because of the high electron affinity of SF_6, low-energy electrons are attached to molecules by resonance capture (within 1 ps) and form metastable association complex $(SF_6)^{-*}$. This also applies to air. It is commonly accepted that the number density of charged particles in gas is controlled by the following governing equation [24]

$$\nabla \cdot \left(-D^{+/-} \cdot \nabla N^{+/-} - N^{+/-} \cdot b^{+/-} \cdot \nabla \varphi\right) = S_{IP} - K_r \cdot N^{+/-} \cdot N^{-/+} \quad (3)$$

where $N^{+/-}$ is the number density of positive/ negative ions, K_r their recombination coefficient, $b^{+/-}$ their mobility, and $D^{+/-}$ their diffusion coefficients.

There has been a considerable amount of work on the measurement of the mobility of negative ions in SF_6 [29-36]. However, the gas pressure used in almost all the measurements was at most a few hundred mbar, much low than the pressure used in GIS or wall bushings. At low pressure the mobility of negative SF_6 ions is around 5×10^{-5} $m^2/V/s$. Schmidt and Jungblut [35] were the first authors to obtain the mobility of SF_6 ions at high pressure from 0.25 bar to 21 bar. They obtained a value of 9×10^{-6} $m^2/V/s$ for both positive and negative SF_6 ions. The mobility remains constant for electric field strength below 10^5 V/m at 0.25 bar and below 6×10^5 V/m at 21 bar. A value of 3.6×10^{-5} $m^2/V/s$ for negative SF_6 ions at 1 bar was obtained by Kindersberger et al [37]. Since the results in [35] were obtained under conditions close to the real application, the value of 9×10^{-6} $m^2/V/s$ is therefore used in the present work.

There is very little work on the measurement of diffusion coefficient of SF_6 ions in their parent background gas. We derived a value of 7×10^{-8} m^2/s from the results given by Nakamura [38] by extrapolating his results to an E/N value corresponding to the case under study (6 bar and 300 K for SF_6). A value of 2.4 for the energy factor, defined as $39.6D/\mu$ where D is the diffusion coefficient of negative ions in SF_6 and μ their mobility, was obtained by Naidu and Prasad [34]. Using the mobility value of 9×10^{-6} $m^2/V/s$ given by Schmidt and Jungblut [35], a diffusion coefficient of 5.45×10^{-7} m^2/s was calculated. Using Einstein's relationship and the mobility of Schmidt and Jungblut, we can also derive a value of 2.3×10^{-7} m^2/s. The closest experiment conditions to the real application were used by Kindersberger et al [37] at 1 bar and room temperature to directly obtain a value of 2.84×10^{-9} m^2/s. It will be shown in Section 4 that diffusion plays an unimportant role in the charge accumulation process. The experimental value of 2.84×10^{-9} m^2/s will be used in our model.

S_{IP} in Equation (3) represents the generation rate of ion pair. For SF_6 we have little experimental results. The only work was done by Kindersberger et al [37] who obtained values from 2.6×10^7 $/m^3/s$ in the ground floor of buildings to 5.5×10^7 $/m^3/s$ outdoor at 4 bar. Their results were extrapolated to 6 bar based on the measured values at different pressures, giving a value of 3.3×10^7 $/m^3/s$, which is used in the present work.

The recombination coefficient of positive and negative SF_6 ions was only measured by Kindersberger [37] at 1 bar with a value of 1.7×10^{-12} m^3/s. Since the recombination coefficient at higher pressure is approximately inversely proportional to pressure, therefore in the present case of 6 bar, the recombination coefficient is estimated as 2.8×10^{-13} m^3/s for use in Section 4.

The electrostatic potential distribution in the gas region is obtained by solving Poisson's equation. The space charge

required is calculated based on the number density of positive and negative ions.

There have been experimental indications that under certain conditions the surface of insulators may conduct a significant proportion of the leakage current [16]. There were also proposals to modify the insulator surface material to change and thus optimize the insulation performance. One way to do this is to form a surface layer of particular conductivity to influence the electric field distribution. According to [17], the surface conductivity on an epoxy insulator lies in the range of 10^{-18} S to 10^{-20} S when the applied field varies from 1 kV/mm to 5 kV/mm.

The thickness of the surface layer is normally negligibly small compared with the diameter of the insulator. It is acceptable to treat the surface layer as a zero-thickness conducting surface satisfying the following conservation rule for current

$$\nabla \cdot (2\pi r\sigma_s \cdot \nabla\varphi_l) = 2\pi r(J_{snor} - J_{gnor}) \quad (4)$$

where φ_l is the electrostatic potential on the surface layer, σ_s is the surface electrical conductivity and $2\pi r(J_{snor} - J_{gnor})$ represents the current entering the surface layer from the gas and solid regions with J_{snor} being the current density in the solid material in the direction normal to the surface and J_{gnor} the corresponding normal current density in the gas region. The current density vector in the gas can be expressed as

$$\boldsymbol{J}_g = e[\boldsymbol{E}(n^+b^+ + n^-b^-) - (D^+\nabla n^+ - D^-\nabla n^-)] \quad (5)$$

2.3 BOUNDARY CONDITIONS AND MESH SIZE

Boundary conditions are essential to obtain reasonable computational results from the governing equations. For convenience Table 1 summarises all boundary conditions required in the present work. The most important consideration is the interaction between solid surface and ions. A solid surface (insulator surface or electrode surface) does not directly generate ions. Therefore, when the ions are subject to an electric force to move away from the surface, their number density will drop at the surface. If the field is strong enough, the ion number density will approach zero. When the electric field near a surface attracts an ion towards it, the ion will collide with the surface. As a result, at least one electronic charge is delivered to the surface through neutralisation of the ion. In reality, the ion must be neutralised on the surface. This is because in the presence of a constant DC field in the normal direction of the surface, a leakage current has to be maintained across the surface by this ion flux but the ions cannot be continuously attached onto the surface.

The model was implemented in COMSOL 5.0. The charge transport equations are implemented using the Coefficient Form PDE interface and the surface layer by Coefficient Form Boundary PDE interface. Care has been taken to ensure the correct computation of the divergence term of the vector quantities that are solved. Despite the friendly user interface in COMSOL to set up multi-physics models, severe convergence difficulties can be experienced due to the dominance of ion drift in strong electric field in gas. A stabilisation method based on artificial diffusion has to be employed to obtain a converged solution to the governing equations. On the other hand, the effect of artificial diffusion has to be negligible to obtain accurate results.

Meshing is an important step in the simulation process to obtain converged results with sufficient spatial resolution. Extensive trial work has led to the choice of a maximum mesh size of 1-3 mm with a refined mesh size of 0.05 mm near the insulator surface or conductors with small curvature radius.

3 VALIDATION OF MODEL

Despite the effort so far there are still uncertainties in the properties of epoxy and gas. Therefore, model validation is essential to build confidence in its effectiveness. In this section, two experimental cases involving different gases and voltage levels are modelled and prediction compared with measurement.

3.1 EPOXY INSULATOR IN AIR AT 15 KV

The first case was from Winter and Kindersberger [21] with an epoxy insulator placed in a test chamber that was filled with air at atmospheric pressure and room temperature. The insulator has a length of 132 mm and diameter of 80 mm. The computational domain in the present work was constructed based on the geometric information given in [21], especially its Figure 1. The material properties used are also identical to those used in their simulation (given in captions of their Figure 9).

The current density of ions in the model consists of three components, the drift current, the physical diffusive current and the artificial diffusive current. The artificial diffusion coefficient of ions is related to the mobility of the ions and a characteristic field strength [39]. This field strength is varied until the solution is converged with a minimum value of the characteristic field strength. It has been found that the ion current density in gas due to artificial diffusion is only 0.3% of the total current density for the case reported in this section. It remains less than 5% when a voltage of up to 800 kV is applied across a wall bushing spacer (section 4.2). The use of false diffusion to stabilize the computation is thus acceptable. A comparison of the electrostatic potential along the surface of the insulator is given in Figure 1. The predicted distribution from the present work is slightly lower than the measurement. This is reasonable since steady state corresponds to a time of infinity. The predicted maximum surface charge density is 1.92×10^{-5} C/m^2 (Figure 2) which compares well with the value of 1.75×10^{-5} C/m^2 given in [21]. The spike in Figure 2 at z = 0.144 is due to the curvature change at that point on the surface.

Despite the very good agreement, our calculated negative ion number density distribution is slightly different from that reported in [21], especially the high-density strip shown in Figure 3. The strip in our case is slightly wider and joins the electrode surface while in [21] it joins the insulator surface.

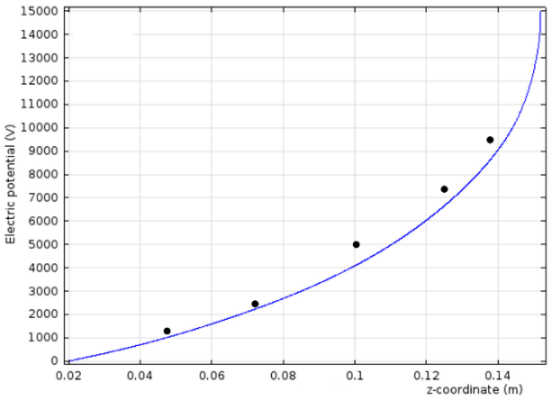

Figure 1 Predicted electrostatic potential distribution along the axial direction on the insulator surface (full curve) and the measured potential values with a voltage application time of 8000 hours at 15 kV as given in [21] (symbols).

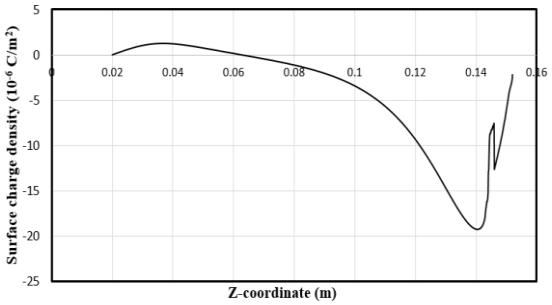

Figure 2 Predicted surface charge density along the axial direction of the insulator for an applied voltage of 15 kV.

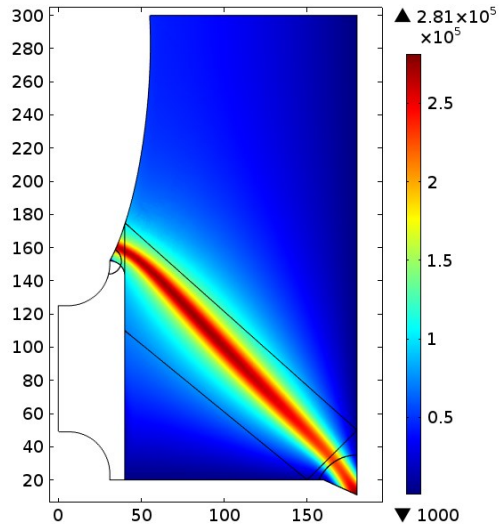

Figure 3 Distribution of the negative ion number density in the gas (air) domain with a pressure of 1bar and applied voltage of 15 kV. The black lines in the gas domain are used to refine the grids. They cannot be removed from the diagram but should be ignored.

3.2 EPOXY INSULATOR IN SF_6 AT 200 KV

The experimental cases in [9] with different insulator shapes were simulated with the conditions given in the experiment. The insulators have a short length of 4 cm and diameter of 4 cm, much smaller than the case in Section 3.1. The pressure of SF_6 is between 2-3 bar. The filler materials are Silica (SiO_2) and Alumina(Al_2O_3). No material properties are given in [9]. The electrical conductivity of epoxy material, in the absence of information provided by the authors, is given a value of 1.89×10^{-16} S/m for epoxy filled with Al_2O_3 microns [40].

The calculated surface charge density is shown in Figure 4 by the dashed lines. It is fairly close to or slightly larger than the measurement averaged in the azimuthal direction (large circules in Figure 4). Our prediction is reasonable because the experimental system approaches steady state in 3 to 5 hours [9]. There is large fluctuation of surface charge density in the azimuthal direction indicating the unevenness of the distribution. In addition, the present model leads to results much closer to the measurement than the simple estimation in [9] which is shown by the solid lines in Figure 4 .

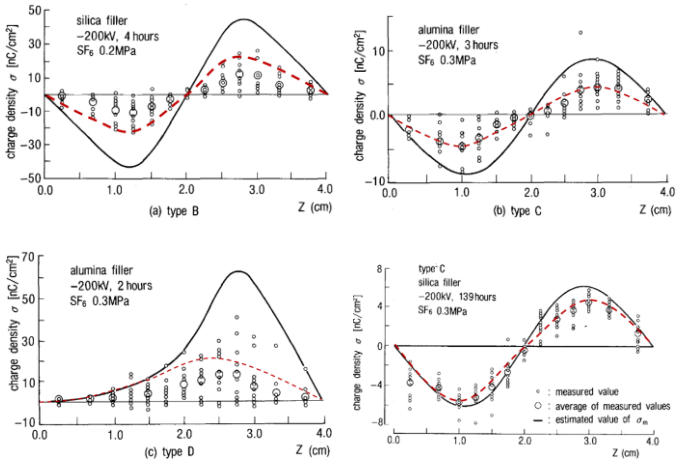

Figure 4 Comparisons of measurement and simulated results. Small circles – measured surface charge density; large circles – average value of the measured charge density in the azimuthal direction; solid curves – from simple model in [9]; red dashed curve – present work.

4 COMPUTATIONAL ANALYSIS OF THE PERFORMANCE OF AN 1100 KV EPOXY SPACER

Following the verification of the charge transport model in Section 3, it was applied to an HVDC epoxy spacer designed for application in wall bushings up to 1100 kV. The original design of the bushing is three dimensional with a length of 28 meters. Due to the prohibitive demand on mesh and computational time, the gas environment for the insulator is simplified. As can be seen in Figure 5, the insulator is mainly stressed between the central conductor and by the earthed wall (Figure 5b) while in the longitudinal direction there is less electrical stress. We are thus able to approximate the gas environment by using a spherical domain of the same diameter of the bushing barrel, as given in Figure 6. In the present work, we use two geometries of the central electrode with the simple one shown in Figure 6. The more complicated geometry will be introduced in Section 4.4 when relevant results are discussed. Unless stated otherwise, all results presented in Sections 4.2 to 4.4 are obtained using an epoxy electrical conductivity of 1.6×10^{-16} S/m (manufacturer supplied value) .

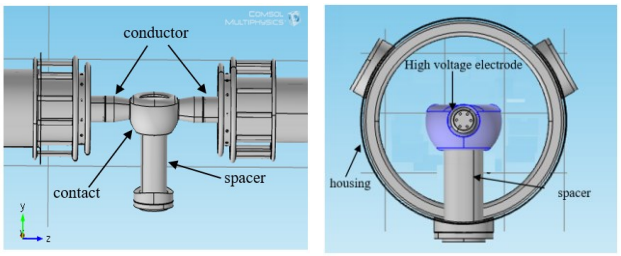

(a) (b)

Figure 5 Front and side view of the original design of the middle section of the wall bushing. The shape of the spacer is for illustration only.

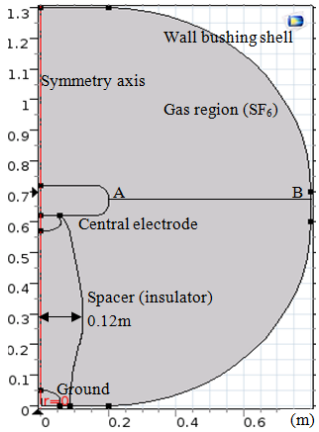

Figure 6 Cross sectional view of the simplified insulator system. The dimensional values are in mm.

The spacer itself is axis-symmetric and two electrodes are embedded into it. The maximum diameter and height are 246 mm and 620 mm, respectively. The original design contains a section of the surface with crest-furrow corrugation to increase the creepage distance. The SF_6 gas is at 6 bar absolute. A temperature of 300 K is used in the present work. The maximum mesh size is 3 mm in regions where electric field is changing slowly in space. A typical mesh size of 0.3 mm is used near the conductor and insulator surfaces to ensure adequate spatial resolution. Further reduction in mesh size leads to negligible change in the solution. Relatively strong relaxation should be used to guarantee convergence of the solution process at very high applied voltages.

4.1 OVERALL FEATURES OF THE CHARGE ACCUMULATION PROCESS AROUND THE SPACER

Charge accumulation is a consequence of charge movement in the insulation media, whether gas or solid. The flux of charge in the epoxy material is proportional to the local electric field strength since the electrical conductivity is fixed. This is however not the case in gas because the electrical conductivity of gas depends on the charge number density and also the mobility. Unlike in epoxy, charges in gas such as SF_6 are allowed to have very different number density depending on the transport mechanisms. Accumulation of charges occurs when the divergence of the initial charge flux is not zero. At the solid surface, it is the difference in charge fluxes in gas and in epoxy in the normal direction that leads to charge accumulation in the absence of a surface layer. In reaching steady state, the accumulated charges alter the potential distribution which adjusts the local normal electric field components in gas and in epoxy to balance the charge fluxes.

The concept of surface layer refers to the situation where the ability of the material near the insulator surface to conduct current is greatly enhanced or very different from the bulk material due to coating, ageing or other surface modification. The thickness of this layer is usually small (<0.1 mm). A surface layer with distributive electrical conductivity provides an additional dimension (along the surface) for the balance of electric currents across the gas-solid interface, therefore helping smoothen (minimize) the electric field strength and surface charge density along the insulator surface.

To explain the phenomenon, a simple case with a fixed low electrical conductivity in SF_6 is simulated (Case A in Figure 7). The electrical conductivity in SF_6 is set to only 1% of that in epoxy. As a result, little current can pass the interface and the current density in epoxy in the tangential direction of the insulator surface is much larger than that in the normal direction. Local enhancement of electric field is observed where the surface is crest and furrow shaped (Case A in Figure 7). Positive charges are accumulated on most of the insulator surface in order to increase the normal field component in gas near the surface to increase the normal current density component (Figure 8). The electrostatic potential along the insulator surface is given in Figure 9.

In Case B, the electrical conductivity of SF_6 is set to a value close to that obtained from the charge transport model in the present work (5.35×10^{-18} S/m). When a smaller value of electrical conductivity for epoxy (3.33×10^{-18} S/m [21]) is used, the gas now becomes more conductive than epoxy and as a result the normal electric field component in epoxy has to be enhanced by accumulated negative charges (Case B in Figure 8) in an attempt to balance the normal current density from the solid. The field strength near the top of the insulator is significantly enhanced (Case B in Figure 7) while on the surface of the lower part of the insulator the field is suppressed. This is linked to the very different potential distribution shown in Figure 9, demonstrating the fact that negative charge accumulation occurs when the gas is more conductive than the solid insulation material.

When the charge transport process is fully considered (Case C), the electric field becomes slightly stronger than Case A. Based on the number density of positive and negative charges and the mobility, we obtain an electrical conductivity of SF_6 in the range from 2.14×10^{-18} S/m to 5.35×10^{-18} S/m. The value at the middle of the insulator surface is 3.0×10^{-18} S/m, which is less than 3% of the epoxy conductivity (1.6×10^{-16} S/m). Therefore, this case is similar to Case A with mainly positive charges accumulated on the surface of the insulator (Case C in Figure 8). The potential curve is also similar to Case A as shown in Figure 9.

It is therefore very clear that the polarity of the charge accumulated on the insulator surface and modification of the surface potential both depend on the relative magnitude of the effective conductivities of epoxy and gas.

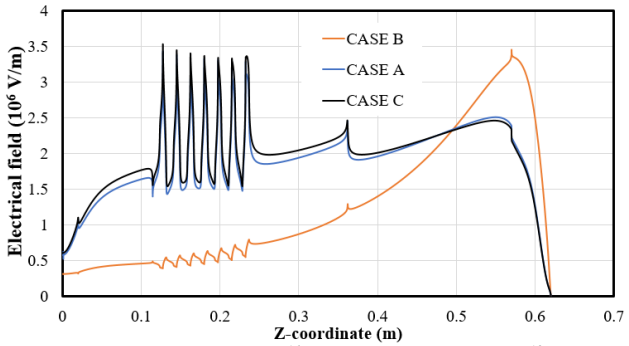

Figure 7 Case A (Blue line): 1.6×10^{-16} S/m for epoxy and 1.6×10^{-18} S/m for SF_6; Case B (Yellow line): 3.33 $\times10^{-18}$ S/m for epoxy and 5.35×10^{-18} S/m for SF_6; Case C (Black line): solution by charge transport model with 1.6×10^{-16} S/m for epoxy, in the gas side;

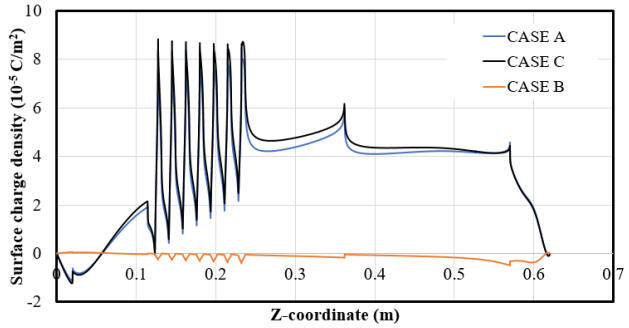

Figure 8 Surface charge density along insulator surface. Case A (Blue line): 1.6×10^{-16} S/m for epoxy and 1.6×10^{-18} S/m for SF_6; Case B (Yellow line): 3.33 $\times10^{-18}$ S/m for epoxy and 5.35×10^{-18} S/m for SF_6; Case C (Black line): solution by charge transport model with 1.6×10^{-16} S/m for epoxy;

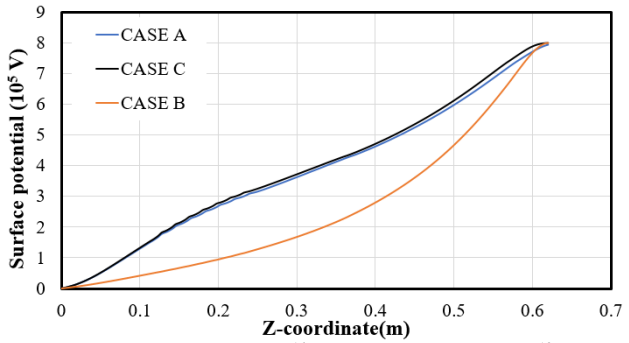

Figure 9 Case A (Blue line): 1.6×10^{-16} S/m for epoxy and 1.6×10^{-18} S/m for SF_6; Case B (Yellow line): 3.33 $\times10^{-18}$ S/m for epoxy and 5.35×10^{-18} S/m for SF_6; Case C (Black line): solution by charge transport model with 1.6×10^{-16} S/m for epoxy.

4.2 NONLINEARITY OF THE SYSTEM

In equilibrium state without any applied electric field, the ion pair number density attains a value of $\sqrt{\frac{S_{IP}}{k_r}}$, which is 1.13×10^{10} m^{-3}. When the ions drift in an applied electric field and with the boundary conditions given in Table 1, the ion number density develops severe non-uniformity in the gas domain, as shown in Figure 10. The maximum value is around 3.6×10^{6} m^{-3}, much lower than the equilibrium value. Positive ions are expelled from the conductor and insulator surface while negative ions are attracted towards the electrode surface. There is a strip of relatively higher negative ion number density as shown by the broken rectangle in Figure 10b. The reduction in ion number density in comparison with the equilibrium value means that without additional ionization sources due to electric discharge near the insulator (corona or partial discharge), the effective electrical conductivity of SF_6 can vary over a few order of magnitude through the change in ion number density. Thus, we must solve the charge transport equation directly to account for current conduction in the gas, instead of using the electrical conductivity.

Figure 11 shows the electrostatic potential distribution along the insulator surface at different applied voltages. The difference between the distribution at 200 kV multiplied by a factor of 4 and that at 800 kV represents the nonlinearity of the system (Figure 11a). This also applies to the surface charge number density in Figure 11b. Examination of the governing equations indicates that it is the recombination terms that contribute to this nonlinearity.

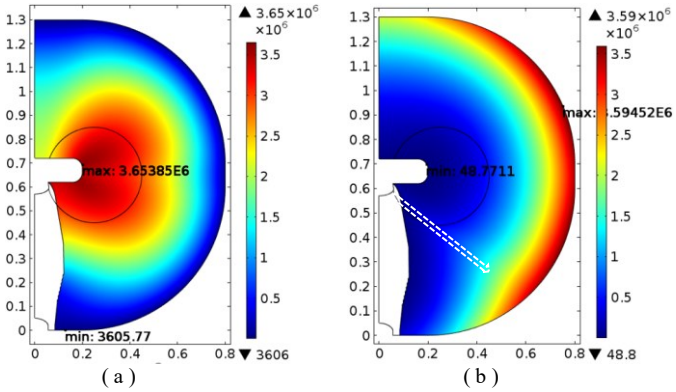

Figure 10 Density distribution of positive (a) and negative (b) SF_6 ions in the gas domain at an applied voltage of 800 kV.

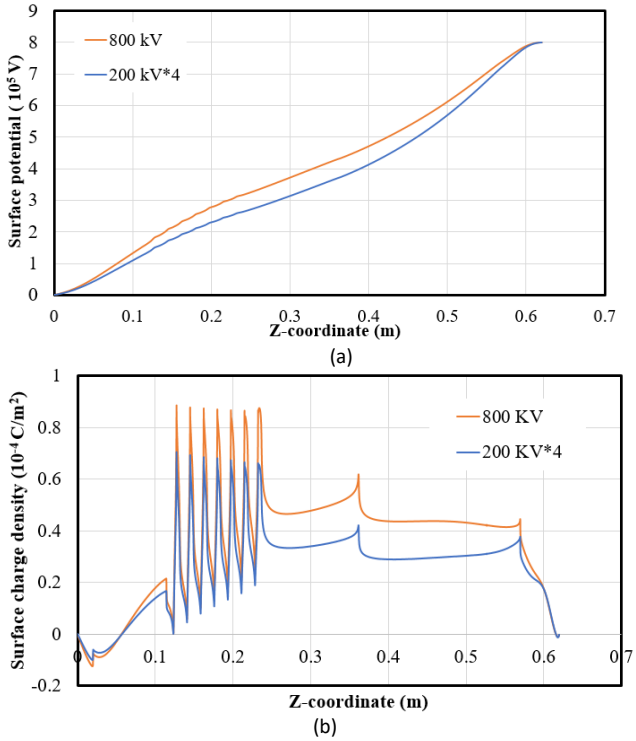

Figure 11 Electric potential distribution (a) and surface charge density (b) along the insulator surface at 200 kV (but with results multiplied by a factor of 4) and 800 kV.

4.3 INFLUENCE OF SURFACE PROFILES ON THE MAGNITUDE OF ACCUMULATED SURFACE CHARGE

Under steady state, the normal electric field component on the gas-solid interface is related to charge accumulation. The field component tangential to the insulator surface is however affected by the total effective conducting cross sectional area normal to the tangential current component. In the original design, the lower part of the insulator has crest-furrow shaped corrugation on its surface. Our modelling results (Case C in Fig. 7) show that this surface profile in fact leads to a maximum electric field strength, 3.5×10^6 V/cm at 800 kV, that is higher than that near the top of the insulator (2.5×10^6 V/cm). In contrast, the field strength with a smooth surface has a lower maximum field strength (Figure 12). It is to be noted that the smoothness of the surface has a significant influence on the peak electric field. The two peaks at z = 0.23 m and z = 0.36 m are due to the sudden change of the surface tangential direction, leading to very small radius of curvature on the surface. Therefore, in practical insulator design and manufacturing, the smoothness of the surface can have a significant effect on the local electric field.

The effective electrical conductivity in SF_6 varies along the insulator surface by a factor of 2. In the absence of a surface layer, minimum surface charging can be achieved if the effective electrical conductivity of the gas is approximately equal to that of the insulator. Ideally, the electrical conductivity distribution of the solid insulation material along the insulator surface should also be optimized based on the effective electrical conductivity of the gas at steady state which can be calculated using the mobility of the ions and ion number densities.

4.4 EFFECT OF SHIELDING OF TRIPLE JUNTION

The triple junction is always a matter of concern in the operation of insulator if it is not well shielded. Results in Figure 13 show that with the shielding cap the total electric field along the surface (Figure 13a) becomes much higher than that with the simple geometry, as given in Figure 13b. With the cap the maximum field strength along the surface appears at a vertical position that is level with the bottom of the cap. It increases from 2.4×10^6 V/m with the simple shape central electrode to 4.4×10^6 V/m with the shielding cap, an increase of 83% (Figure 12a). Much more negative charges are accumulated on the surface in this region as well.

A close examination reveals that in the present case the electrical conductivity of epoxy is 1.6×10^{-16} S/m (manufacturer supplied value) which is much larger than the effective electrical conductivity of SF_6 which is in the range of 2.14×10^{-18} S/m to 5.35×10^{-18} S/m. Thus, epoxy is much more conducting than SF_6 and the gas gap between the inner downwards side of the cap and the upper part of the insulator is exposed to a high potential and the electric field is thus enhanced. The electric field vector given in Figure 14a indeed shows that there is a dominant normal electric field at the surface in the upper part of the insulator. With a higher epoxy electrical conductivity, the idea of using this shielding cap does not suppress the electric field, instead it enhances the field strength which is not favored.

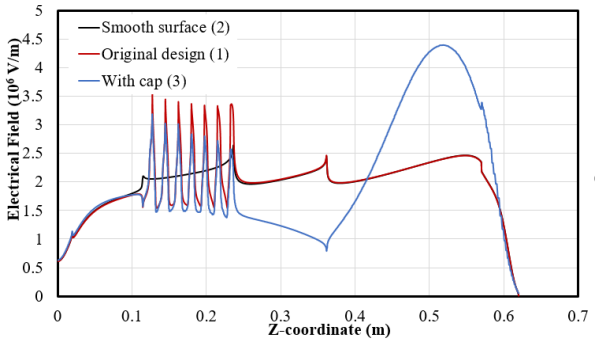

(a) Electric field

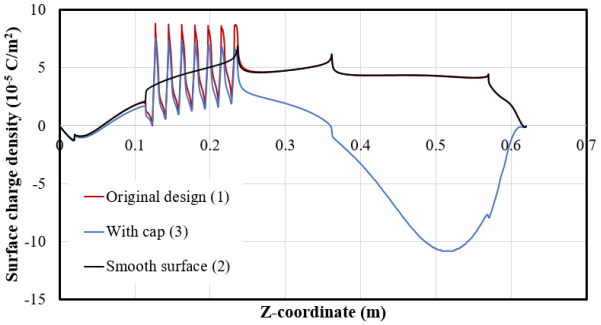

(b) Surface charge density

Figure 12 Electric field strength (total field) (a) and surface charge density (b) at the insulator surface for three cases: original design (1); crest-furrow corrugation replaced by smooth surface (2), and central conductor replaced by a cap (3).

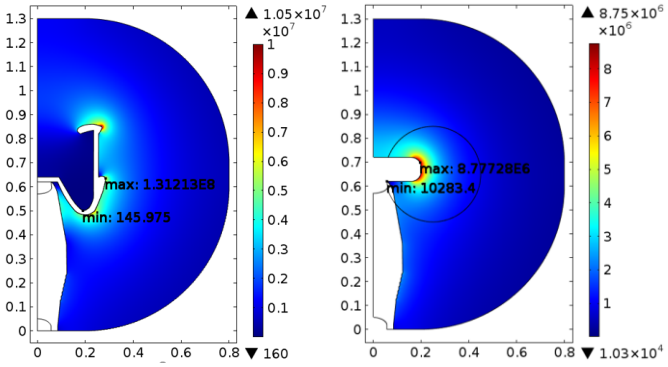

Figure 13 Electric field strength distribution in the gas domain with a shielding cap for the insulator at 800 kV.

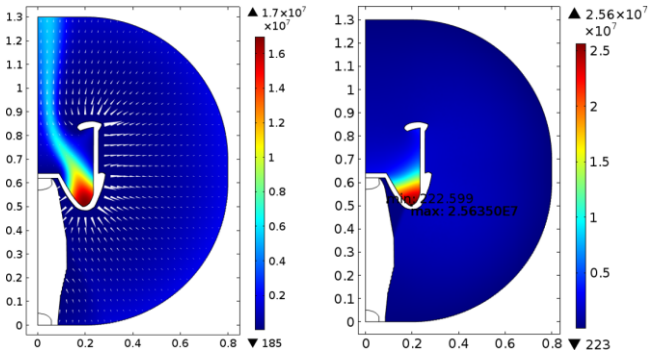

(a) (b)

Figure 14 Positive (a) and negative (b) ion number density distribution in the gas domain with the shielding cap on the high voltage side of the insulator. The applied voltage is 800 kV.

Computation was also performed at 200 kV and 1100 kV for the insulator with the shielding cap. The distribution of ion number density is similar to Figure 14. Results in Figure 15 and 16 show that at all three voltage levels the use of the shielding cap greatly enhances the local electric field near the top of the insulator. The maximum electric field at the upper-outer edge of the cap has a value of 2.5×10^7 V/m at 1100 kV. The maximum electric field along the insulator surface is 6×10^6 k/m, as shown in Figure 15. Compared with the 800 kV case with the central electrode as shown in Figure 10, there is a much larger amount of negative charge accumulated on the insulator surface, therefore changing the local potential distribution and also local electric field on the surface.

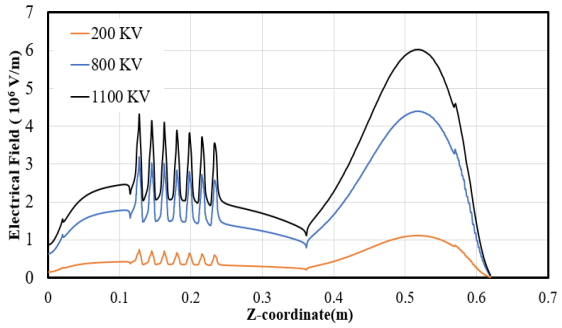

Figure 15 Electric field on the insulator surface at three applied voltages of 200 kV, 800 kV and 1100 kV with the shielding cap.

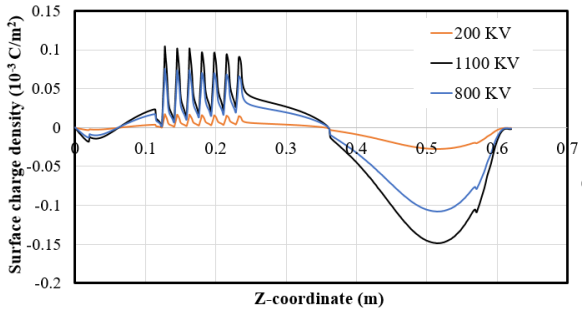

Figure 16 Surface charge density distribution at three applied voltages of 200 kV, 800 kV and 1100 kV with the shielding cap.

4.5 PRACTICAL FACTORS THAT AFFECT THE INSUATION PERFORMANCE OF INSULATORS

The present study assumes that there are no additional ionization mechanisms present in the system under study. This includes any partial discharges or corona near the insulator. The authors have performed measurement of the potential near the insulator surface under HVDC stress in SF_6 with the experimental setup illustrated in Figure 17. The insulator has a metallic insertion at each end which has a depth of 20 mm and a diameter of 20 mm. The disk electrodes (labeled 1 and 3 in Figure 18(b)) are connected to the insulator through a bolt. The insulator has an overall length of 150 mm and diameter of 50 mm at one side (near disk 1) and 55 mm at the other side (disk 3). The diameter of the disk electrodes is 100 mm. The left-hand side disk (disk 3) is earthed.

The electrostatic potential probe used in the present work is Trek 6000B5C with a matching conversion circuit (Model 347). It has a measurement range of 0 – 3000 V, DC. The sensing head has a diameter of 11.2 mm, corresponding to a spatial resolution better than 5.6 mm. The sensor was parked at a shielded location (on the left hand side of disk 3 in Figure 18(b)) when high voltage was applied. On completion of the voltage application, the high voltage was reduced to zero and the feeder wires earthed. The two disks on the high voltage side (disk 1 and 2) were then separated physically to provide physical insulation from the voltage source. Thus the high voltage end of the insulator is floating during the measurement process. The probe was then moved towards the insulator for potential measurement. The output of the probe at the measurement locations has been calibrated against a standard HVDC voltage source (0.1% accuracy) which is connected to a thin strip of conducting foil tightly attached to the insulator surface.

Before sealing the chamber for high voltage test, an ultraviolet camera was used to identify locations of significant partial discharges in air. It was found that the connection part between the high voltage disk electrode (disk 1) and metallic insulator insertion was causing severe partial discharges. The surface near the connection was then cleaned and the insulator realigned with the disk electrodes 1 and 3. The second location for partial discharge in air (when the chamber was opened) was near the edge of the high voltage disk electrode. Partial discharges were not detected using PD detectors after the chamber was sealed and filled with SF_6 at higher pressure.

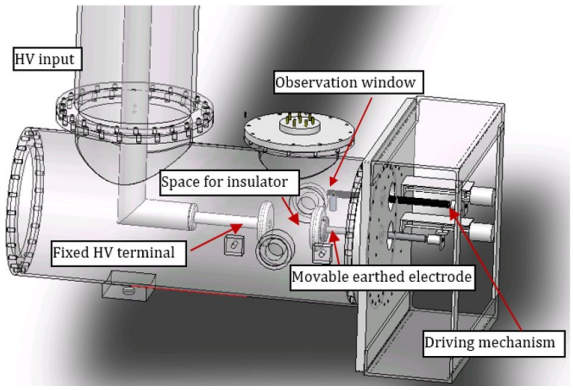

Figure 17 Schematic diagram of the experimental arrangement for insulator surface potential measurement.

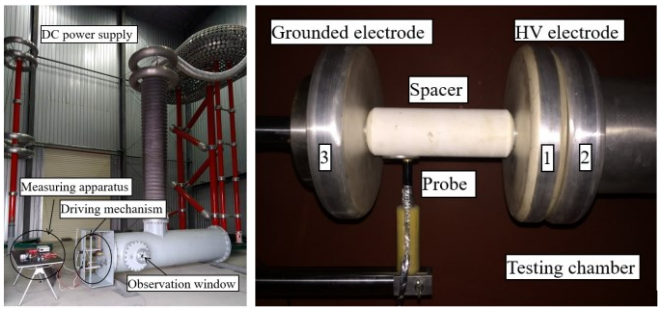

(a) (b)

Figure 18 (a) DC power supply and test chamber and (b) Experimental arrangement of the electrode, epoxy insulator and probe. The filling gas is SF_6 at 6 bar absolute. On finishing the application of a high voltage, disk electrode labelled 1 is driven leftwards to separate from disk 2.

Table 2. Experimental sequence for epoxy insulator in SF_6 with a pressure of 4.1 bar (absolute). The environmental temperature is 10ºC. Electrostatic potential measurement was taken after each voltage application. T_{ind} is the number of voltage application and the duration of each electrical stress. T_{total} is the cumulative voltage application time.

Test ID	HVDC (kV)	T_{ind} (hour)	T_{total} (hour)	Typical results at the end of each group of voltage application.
1	+200	2×0.5	1.0	Maximum of -30 V, 45 mm from the earthed end of the insulator.
2	+300	2×0.5	2.0	Maximum of 20 V, at 35 mm from the high voltage end.
3	+400	4×1.0	6.0	-200 V at 55 mm from the high voltage end, Figure 19(b).
4	+450	3×1.0	9.0	Figure19 (a). Measurement taken per hour.
5	+300	1×9.0	18.0	Figure19 (b).

Two insulators of the same type and dimensions were used in the experiment. The first experiment was aimed at a study of the effect of surface charge accumulation over a duration of 10-20 hours. The filling pressure of SF_6 is 4.1 bar absolute. The experimental sequence is given in Table 2. The insulator was first stressed with a DC voltage of 200 kV for 1 hour and 300 kV for another hour. Measurement of the surface potential shows that at the end of this 2-hour DC stress the potential has a maximum value of 30 V at a location that is 35 mm away from the high voltage disk electrode. This is in clear contrast to the situation with a pressure of 1.01 bar (absolute) where the surface charge accumulated in 1 hour at 200 kV induces a potential of 300 V – 400 V. To investigate the effect of the magnitude of the applied DC voltage, it was then increased to 400 kV for 4 hours and 450 kV for another 3 hours. The surface potential corresponding to DC voltage of 450 kV was measured each hour as shown in Figure 19(a). In Figure 19, the earthed end of the insulator has an axial coordinate of 286 mm and the high voltage end has a value of 436 mm, giving an insulator length of 150 mm. Results show that at a DC voltage of above 400 kV, a significant amount of negative charges were already accumulated within 7 hours (4 hours at 400 kV and 3 hours at 450 kV), near the high voltage electrode (Figure 19(a)). Thus another 9-hour long electrical stress at 450 kV was applied to observe the further potential variation. The results are given in Figure 19(b). It must be noted that the measured potential is induced by the charges on the insulator only because the DC power supply was switched off and isolated from the insulator during measurement. This is different from the case in [21] where the potential was measured while the HV was applied. It is evident that the increased negative potential from -200 V to -400 V on the HV electrode side is induced by increased negative charge density accumulated on the insulator surface. The pocket of negative charges (arrowed lines) moves with an approximate speed of 3 mm/hour. More positive charges are accumulated near the earthed electrode, increasing the potential from 50 V to 200 V.

In practice, there is always unevenness of the surface charge density in the azimuthal direction of the insulator due to various reasons, such as the presence of ionization source at locations away from the insulator due to discharge or due to the initial presence of surface charge in the installation stage. The results in Figure 20 were obtained with another insulator of the same size and material. In this experiment the insulator was rubbed with a piece of dry cleaning paper after its installation and the resultant potential distribution along axial lines of different azimuthal angle was measured after sealing the chamber and filling it with SF_6 at 4.1 bar absolute. Results are presented in Figure 20. It is clear that there is large variation of surface charge density or potential in the azimuthal direction and negative charges are dominant. After the application of 400 kV for 1.5 hours and 450 kV for another hour, the potential distribution has had substantial adjustment as shown by the curves labelled "before 8h" in Figure 21 with the following features:

- With the initial charge on the surface, positive surface potential can be induced on the application of 450 kV DC voltage.
- The surface potential after 2.5 hours still bears memory of the initial charge. This can be evidenced by comparing the potential distribution at 120º of azimuthal angle in Figure 21(b) with the corresponding curve in Figure 20.
- Despite the dominant positive potential along the insulator surface, there is a general tendency of accumulation of negative charges near the high voltage electrode which induce a potential drop beyond the position of 400 mm, except at 120º.

To further understand the charge accumulation process, a 9-hour long application at the same voltage of 450 kV was performed and the results are given in Figure 21 by curves labelled as "after 9h". It is shown that more and more negative charges are accumulated near the high voltage end of the insulator, significantly reducing the potential over half of the insulator length. The two curves in Figure 21b show, in particular, that a pocket of negative charge (at 330 mm) can stay on the surface for over 8 hours without being dissipated.

The above discussion of the experimental results points to the conclusion that in practical situations with possible minor defects of the insulator body, for an insulator of such size steady state at 450 kV will not be reached within 24 hours following the application of the high voltage. This is further supported by the result given in Figure 22 showing that at atmospheric pressure in SF_6 charge decay over 11 hours only leads to a 31% reduction of the peak voltage, giving a decay time constant of around 30 hours.

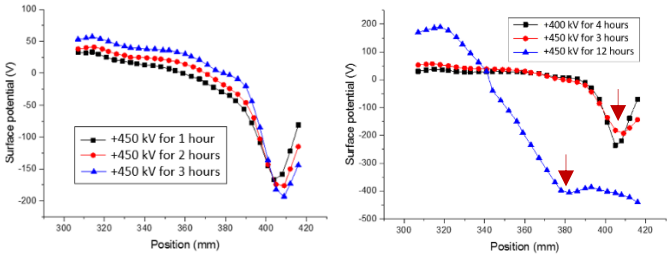

(a) (b)

Figure 19 (a) Surface potential distribution in the axial direction for a period of 7 hours of electrical stress, 4 hours at 400 kV and 3 hours at 450 kV. (b) Comparison of cumulative surface potential distributions corresponding to voltage application of 4 hours at 400 kV, 3 hours at 450 kV and 12 hours of 450 kV. SF_6 gas is at a pressure of 4.1 bar. More details are given in Table 2.

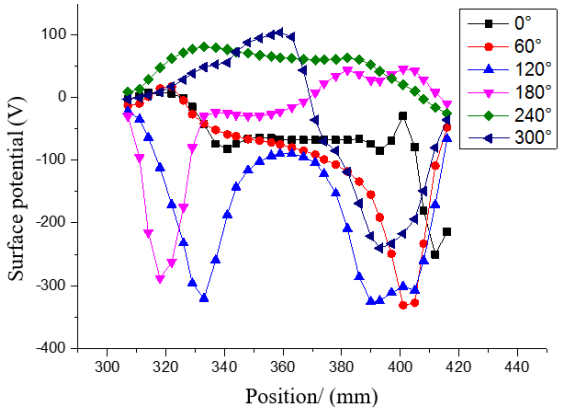

Figure 20 Initial distribution of potential near the insulator surface after the insulator was rubbed with a piece of dry paper after its installation but before sealing the chamber.

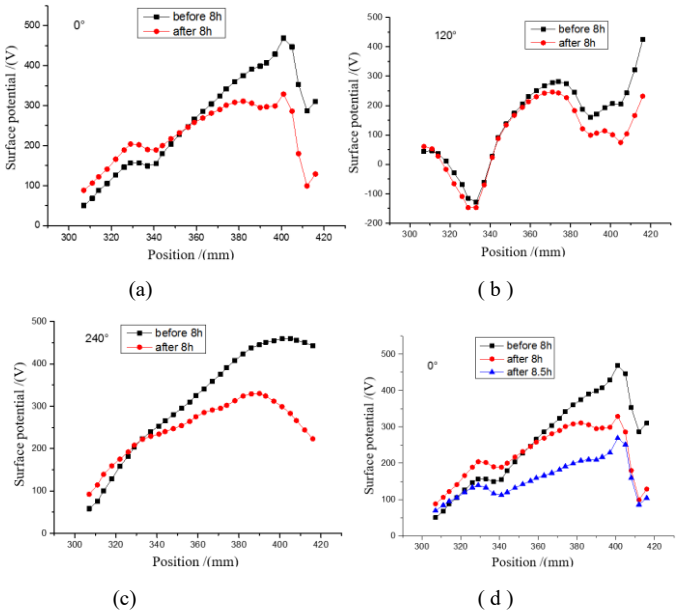

Figure 21 Comparison of the ppotential distribution along the axial direction of the insulator before and after the application of 450 kV for a continuous period of 8 hours. This means that the curve labelled with "before 8h" is the cumulative result of 1.5 hours at 400 kV and 1 hour at 450 kV. Diagram (d) is a repeated measurement at 0° to check the repeatability of the measurement results.

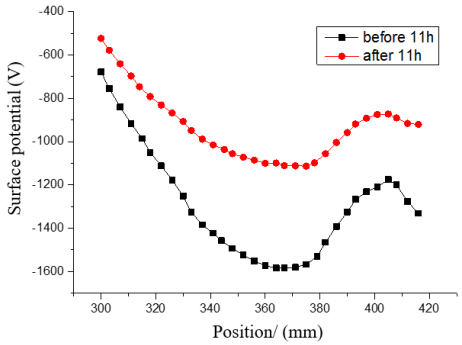

Figure 22 Electrostatic potential variation near the surface of the first insulator over a period of 11 hours from an initial condition which was created by breakdown of the electrode gap in SF_6 at 1.01 bar absolute with an applied voltage of -325 kV. Measurement was taken at the azimuthal angle of 0°.

5 CONCLUSIONS AND FUTURE WORK

A charge transport model based on ion drift and diffusion in gas has been detailed in the present work with discussions on its model parameters, boundary conditions and influence of mesh size. It has been verified by experimental results in different gases and at different voltage levels. All model parameters are carefully examined based on literature research and wherever possible measured values are used. The following conclusion can be arrived at based on the present work:

- In strong electric field the number density distribution of charged particles in the gas is non-uniform and varies by several orders of magnitude. The concept of electrical conductivity as a material property becomes invalid;
- The polarity of accumulated surface charge depends on the relative largeness of the effective electrical conductivity in gas and in solid insulation material near the insulator surface. When the gas has a much lower electrical conductivity, positive charges will appear on most of the insulator surface with positive polarity.
- The system is nonlinear due to the ionization and recombination of ions. Its effect increases with the applied voltage.
- Shielding of the triple junction can induce strong side effect by increasing the total field strength locally near the edge of the cap if its shape is not optimized.

In practice, there are factors that affect the usefulness of the model. Firstly, in different situations the model parameters such as the bulk electrical conductivity of the insulator material and the mobility of ions may vary. Further effort will be needed to obtain more accurate model parameters. Secondly, localized partial discharge can never be eliminated completely in GIS or wall bushings. This acts as additional ionization sources. Thirdly, experiments have shown that there can exist minor insulator defects due to manufacturing or installation. As a result, the distribution of surface charge can be tremendously non-uniform in the azimuthal direction, making model prediction more difficult. Therefore, much more effort is to be devoted to obtain accurate charge and potential measurement under well-defined experimental conditions, including the measurement of the model parameters. With more powerful computing power, three-dimensional model will be preferred.

6 REFERENCE

[1] K. R. Padiyar, *HVDC Power Transmission Systems: Technology and System Interactions*, New Age International, Inc., India, 1990, Chapter 2.
[2] L. Cheng, H. Feng, and J. He, "HVDC Development and its Reliability in China." IEEE Power and Energy Society General Meeting (PES), Vancouver, Canada, pp. 1-5, 2013.
[3] D. V. Hertem, O. G. Bellmunt and J. Liang, *HVDC Grids: For Offshore and Supergrid of the Future*, John Wiley & Sons, Inc., New York, 2016.
[4] R. Rudervall, J. P. Charpentier and R. Sharma, "High Voltage Direct Current (HVDC) Transmission Systems Technology Review Paper", Energy Week, pp. 2-5, *2000*.

[5] A. Kalair, N. Abas and N. Khan, “Comparative Study of HVAC and HVDC Transmission Systems”, Renewable and Sustainable Energy Reviews, Vol. 59, pp.1653-1675, 2016.
[6] C.M. Cooke, “Charging of Insulator Surfaces by Ionization and Transport in Gases”, IEEE Trans. Electr. Insul., Vol. EI-17, pp.172-178, 1982.
[7] T. Nitta, Y. Shibuya, Y. Fujiwara, Y. Arahata, H. Takahashi and H. Kuwahara, “Factors Controlling Surface Flashover in SF_6 Gas Insulated Systems”, IEEE Trans. Power App. Syst., Vol. PAS-97, pp.959-968, 1978.
[8] V. V. Akimov, V. N. Varivodov and E. K. Volpov, “An Approach to the Spacer Design of HVDC SF_6 Gas Insulated Equipment.”, Proceedings of the 3rd International Conference on Properties and Applications of Dielectric Materials, pp. 525-528, 1991.
[9] H. Fujinami, T. Takuma, M. Yashima and T. Kawamoto, “Mechanism and Effect of DC Charge Accumulation on SF_6 Gas Insulated Spacers”, IEEE Trans. Power Del., Vol. 4, pp. 1765-72, 1989.
[10] S. Kumara, Y. V. Serdyuk and S. M. Gubanski, “Charging of Polymeric Surfaces by Positive Impulse Corona”, Trans. Dielectr. Electr. Insul., Vol. 16, pp. 726-733, 2009.
[11] S. Kumara, S. Alam, I. R. Hoque, Y. V. Serdyuk and S. M. Gubanski, “DC Flashover Characteristics of a Polymeric Insulator in Presence of Surface Charges”, IEEE Trans. Dielectr. Electr. Insul., Vol 19, pp. 1084-1090, 2012.
[12] F. Wang, Y. Qiu, W. Pfeiffer and E. Kuffel, “Insulator Surface Charge Accumulation under Impulse Voltage”, IEEE Trans. Dielectr. Electr. Insul., Vol. 11, pp. 847-54, 2004.
[13] M. T. Gençoğlu and M. Cebeci, “The Pollution Flashover on High Voltage Insulators”, Electric Power Systems Research, Vol. 78, pp. 1914-21, 2008.
[14] R. Sundararajan and R. S. Gorur, “Effect of Insulator Profiles on DC Flashover Voltage under Polluted Conditions. A Study using a Dynamic Arc Model”, IEEE Trans. Dielectr. Electr. Insul., Vol. 1, pp. 124-132, 1994.
[15] H. C. Miller, “Surface Flashover of Insulators”, IEEE Trans. Dielectr. Electr. Insul., Vol. 24, pp. 765-786, 1989.
[16] T. Hasegawa, T. Fujiwara, H. Ooi, S. Yanabu, H. Aoyagi and Y. Kanno, “The Influence of Charging of GIS Epoxy Insulator on DC/Impulse Superposed Breakdown Characteristics”, Gaseous Dielectrics, Vol. VII, pp. 511-518, 1994.
[17] K. Nakanishi, A. Yoshioka, Y. Arahata and Y. Shibuya, “Surface Charging on Epoxy Spacer at DC Stress in Compressed SF_6 Gas”, IEEE Trans. Power App. Syst., Vol. PAS-102, pp. 3919-3927, 1983.
[18] T. Jing, P. H. F. Morshuis and F. H. Kreuger, “Mechanisms of Surface Charge Accumulation in SF_6”, Archiv fur Elektrotechnik, Vol. 77, pp. 151-155, 1994.
[19] S. Sato, W. S. Zaengl and A. Knecht, “A Numerical Analysis of Accumulated Surface Charge on DC Epoxy Rrsin Spaces”, IEEE Trans. Electr. Insul., Vol. EI-22, pp. 333-340, 1987.
[20] T. Hasegawa, T. Fujiwara, H. Ooi, F. Endo, T. Rokunohe and T. Yamagiwa, “Charging and Breakdown Characteristics of Various Surface-Treatment Spacers Under DC Voltage in SF_6”, Gaseous Dielectrics, Vol. VII, pp. 503-509, 1994.
[21] A. Winter and J. Kindersberger, “Transient Field Distribution in Gas-solid Insulation Systems under DC Voltages”, IEEE Trans. Dielectr. Electr. Insul., Vol. 21, pp. 116-128, 2014.
[22] B. Lutz and J. Kindersberger, “Surface Charge Accumulation on Cylindrical Polymeric Model Insulators in Air: Simulation and Measurement”, IEEE Trans. Dielectr. Electr. Insul., Vol. 18, pp. 2040-2048, 2011.
[23] N. Wiegart, L. Niemeyer, F. Pinnekamp, W. Boeck, J. Kindersberger, R. Morrow, W. Zaengl, M. Zwicky, I. Gallimberti and S. A. Boggs, “Inhomogeneous Field Breakdown in GIS-the Prediction of Breakdown Probabilities and Voltages. II. Ion Density and Statistical Time Lag”, IEEE Trans. Power Del., Vol. 3, pp. 931-938, 1988.
[24] U. Straumann, M. Schuller and C. M. Franck, “Theoretical Investigation of HVDC Disc Spacer Charging in SF_6 Gas Insulated Systems”, IEEE Trans. Dielectr. Electr. Insul., Vol. 19, pp. 2196-2205, 2012.
[25] R. Gremaud, M. Hering, P. Simka, C. B. Doiron, M. Baur, V. Teppati, B. Källstrand, K. Johansson, J. Speck, and S. Großmann, “Solid-Gas Insulation in HVDC Gas-Insulated System: Measurement, Modeling and Experimental Validation for Reliable Operation”, CIGRE Session, Paris, French, 2016.
[26] R. Gremaud, M. Schueller, C.B. Doiron, U. Riechert, U. Straumann, and C.M. Franck, “Experimental Validation of Electric Field Modelling in DC Gas-Insulated System”, CIGRE Session, Rio de Janeiro, Brazil, pp.1-8, 2015.
[27] B. S. Guru and H. R. Hiziroglu, *Electromagnetic Field Theory Fundamentals*, Cambridge University Press, Inc., England, 2004.
[28] E. Volpov, “Electric Field Modelling and Field Formation Mechanism in HVDC SF_6 Gas Insulated Systems”, IEEE Trans. Dielectr. Electr. Insul., Vol. 10, pp. 204-215, 2003.
[29] L. G. Christophorou and R. J. Van Brunt, “SF_6/N_2 Mixtures: Basic and HV Insulation Properties”, IEEE Trans. Dielectr. Electr. Insul., Vol. 2, pp. 952-1003, 1995.
[30] I. A. Fleming and J. A. Rees, “The Drift Velocities of Ions in Sulphur Hexafluoride”, Journal of Physics B: Atomic and Molecular Physics. Vol. 2, pp. 777-779, 1969.
[31] D. T. Blair, B. H. Crichton, F. J. Al-Kindi and T. L. Sharma, “Drift Velocities of Positive Ions and Negative Ions in Cylinder SF_6”, Journal of Physics D: Applied Physics. Vol. 22, pp. 755-758, 1989.
[32] F. Li Aravena and M. Saporoschenko, “Mobilities of Positive Ions in Sulfur Hexafluoride Gas”, The Journal of Chemical Physics, Vol. 98, pp. 8888-8891, 1993.
[33] P. L. Patterson, “Mobilities of Negative Ions in SF_6”, The Journal of Chemical Physics, Vol. 53, pp. 696-704, 1970.
[34] M. S. Naidu and A. N. Prasad, “Mobility and Diffusion of Negative Ions in Sulphur Hexafluoride”, Journal of Physics D: Applied Physics, Vol. 3, pp. 951-956, 1970.
[35] W. F. Schmidt and H. Jungblut, “Ion Mobility and Recombination in Compressed Sulphur Hexafluoride”, Journal of Physics D: Applied Physics. Vol. 12, pp. L67-L70, 1979.
[36] J. Winkelmann, “Diffusion of Sulfur Hexafluoride”, Gases, Liquids and their Mixtures, Springer Berlin Heidelberg, pp. 121-124, 2007.
[37] J. Kindersberger, N. Wiegart and S. A. Boggs, “Ion Production Rates in SF_6 and The Relevance of to Gas-Insulated Switchgear”, Annual Report, Conference on Electrical Insulation & Dielectric Phenomena, pp. 123-129, 1985.
[38] Y. Nakamura, “Transport Coefficients of Electrons and Negative Ions in SF_6”, Journal of Physics D: Applied Physics, Vol. 21, pp. 67-72, 1988.
[39] Multiphysics COMSOL, "Reference Manual for Version 4.4”, pp. 162-168, 2013.
[40] S. Singha and M. J. Thomas, “Dielectric Properties of Epoxy Nanocomposites”, IEEE Trans. Dielectr. Electr. Insul., Vol. 15, pp. 12-23, 2008.

Qingying Liu was born in China in 1992. She received the B.Sc. degree from Huazhong University of Science and Technology, Wuhan, in 2013. She is a Ph.D student at the University of Liverpool working in the area of charge accumulation and its effect on the dielectric behavior of insulators under HVDC stress.

J D Yan received the BEng and MEng degrees from Tsinghua University in 1986 and 1988, respectively. He obtained the PhD degree at the University of Liverpool in 1998. Since then he has been working in the University of Liverpool and currently Reader in Electrical Engineering. His research interests include switching arcs, plasma physics, SF_6 replacement and, more recently, HVDC insulation.

Bo Zhang was born in China in 1985. He received the M.Sc. degree from Chongqing University in 2010. Since then he has been working as an engineer in Pinggao Group Co. Ltd in China. His research interests include HVDC insulation and design of HVDC wall bushing.

Liucheng Hao received the BEng and MEng degrees in 2000 and 2004 respectively. He is now a part time PhD student at Xi'an Jiaotong University and Deputy Head of the Technology Centre of Pinggao Group Co. Ltd in China. His research interests mainly focus on insulation technology for high-voltage switchgear and HVDC wall bushings.

Shan Liu was born in China in 1988. He received the B.Sc. degree from Xi'an Jiaotong University in 2011. He is now working as a Ph.D student in Tsinghua University. His research focuses on space charge measurement and insulation behavior of polymer materials under DC stress.

Table 1 Details of boundary and interface conditions used in the charge transport model.

Equation	Boundary description	Conditions
Gas domain, Poisson's Equation	Live electrode surface bounding the gas domain	Fixed value condition at the given DC voltage is imposed.
	Earthed metallic wall	A zero potential is imposed.
	Interface between gas and surface layer	$\varphi_g = \varphi_l$
	Interface between solid and gas (no surface layer)	$\varphi_g = \varphi_s$
Gas domain, positive ion, Equation (3)	All solid surfaces (live electrode, insulator and earthed metallic wall)	Perfect absorber when $\vec{n} \cdot \overrightarrow{E_g} > 0$ (*); Perfect repeller ($n^+ = 0$) when $\vec{n} \cdot \overrightarrow{E_g} < 0$
Gas domain, negative ion, Equation (3)	All solid surfaces (live electrode, insulator and earthed metallic wall)	Perfect absorber when $\vec{n} \cdot \overrightarrow{E_g} < 0$ (*); Perfect repeller ($n^- = 0$) when $\vec{n} \cdot \overrightarrow{E_g} > 0$
Insulator body, Equation (1)	Live electrode surface bounding the insulator domain	Fixed value condition at the given DC voltage is imposed.
	Earthed electrode	A zero potential is imposed.
	Interface with surface layer	$\varphi_s = \varphi_l$ is imposed;
	Interface directly with gas domain (no surface layer)	$-e\left[\boldsymbol{E_g}(n^+b^+ + n^-b^-) - (D^+\nabla n^+ - D^-\nabla n^-)\right] \cdot \overrightarrow{n_s}$ is imposed as the current density into the solid domain. $\overrightarrow{n_s}$ is the unit normal vector on the solid domain boundary.
Surface layer, Equation (5)	Live electrode bounding the top end of the surface layer	Fixed value condition at the given DC voltage is imposed.
	Earthed electrode	A zero potential is imposed.
All equations	On symmetric axis of the domain	The radial derivative of all solved quantities is zero.

(*) $\vec{n}$ is an outgoing unit normal vector from the boundary face of a domain. For example, on the live electrode surface of the gas domain, the unit normal vector points out from the gas domain (going into the live electrode). **Eg** as a vector is the electric field vector in the gas domain.